FZJ-IKP(Th)-1999-26

Abstract

NUCLEAR-MEDIUM MODIFICATION OF THE $\rho^0(1S)$- AND $\rho'(2S)$-MESONS IN COHERENT PHOTO- AND ELECTROPRODUCTION: COUPLED CHANNEL ANALYSIS

N.N. Nikolaev[1], J. Speth[1] and B.G. Zakharov[2]

[1]*Institut für Kernphysik, Forschungszentrum Jülich, D-52425 Jülich, Germany*

[2]*Landau Institute for Theoretical Physics, GSP-1, 117940, Kosygina Str. 2, 117334 Moscow, Russia*

Abstract

We study medium modifications of the the e^+e^- and/or $\mu^+\mu^-$ mass spectrum in coherent photo- and electroproduction of the $\rho^0(1S)$- and $\rho'(2S)$-meson resonances on nuclear targets. The analysis is performed within the coupled $\rho^0(1S), \rho'(2S), ...$ channel formalism in which nuclear modifications derive from the off-diagonal rescatterings. We find that the effect of off-diagonal rescatterings on the shape of the e^+e^- mass spectrum in the $\rho^0(1S)$-meson mass region is only marginal but is very important in the $\rho'(2S)$ mass region. The main off-diagonal contribution in the $\rho'(2S)$ mass region comes from the sequential mechanism $\gamma^* \to \rho^0(1S) \to \rho'(2S)$, which dominates the $\rho'(2S)$ production for heavy nuclei. Our results show also that in the $\rho'(2S)$ mass region there is a considerable effect of the interference of the Breit-Wigner tail of $\rho^0(1S)$-meson with the $\rho'(2S)$-meson.

1 Introduction

The in-medium modification of hadrons in the cold nuclear matter and hot QCD medium has been under active investigation during the last years. In particular, there was considerable interest in the medium effects for light vector mesons. In several papers the masses of vector mesons at rest in nuclear matter have been calculated within different approaches [1, 2, 3, 4, 5, 6, 7]. The in-medium effects for moving vector mesons have been discussed in refs. [8, 9, 10, 11, 12]. Recall that in optics medium effects are described by the refraction index which for the dilute media is calculable in terms of the photon-atom forward scattering amplitude. Extension of this formalism to fast vector mesons with the wavelength $\lambda = 1/p$ much shorter than separation of nucleons in the nuclear matter gives the in-medium mass shift and collisional broadening the form ([8], for the related early works see [13, 14])

$$\Delta m_V(E) = -2\pi \frac{n_A}{m_V} \mathrm{Re} f(E) \ , \qquad \Delta\Gamma_V(E) = \frac{n_A}{m_V} p\sigma(E) \ , \tag{1}$$

where E and m_V are the meson energy and in-vacuum mass, $f(E)$ is vector meson-nucleon forward scattering amplitude and n_A is the nuclear matter density. These formulas are quite general and must hold for any particle in an infinite medium if the inelastic rescatterings and/or coupled-channel effects can be neglected, see below. An experimental observation of the in-medium mass shift and collisional broadening (1) would be very interesting. Potentially it could give information on the VN scattering amplitude which cannot be measured directly.

In order for the mass shift and collisional broadening (1) to be observed experimentally the typical decay length $L_d \sim E/m_V\Gamma_V$ must be smaller than the nucleus radius R_A, i.e., the momentum of the vector meson must be smaller than

$$p_\rho < 6 \text{ GeV}, \quad p_\omega < 300 \text{ MeV}, \quad p_\phi < \ 200 \text{ MeV} \, , \tag{2}$$

for the ρ^0-, ω^0-, and ϕ^0-meson, respectively [8]. Thus only for the ρ^0-meson [1] there is a sufficiently broad energy interval where the relations (1) could be used.

The applicability limits (2) are purely kinematical ones and do not take into account possible interference of decays of the vector meson inside and outside the target nucleus and the quantum effects in production of the vector mesons. The both effects were studied, and found to be important, in the recent [10] Glauber-Gribov multiple-scattering theory [15, 16] analysis of coherent ρ^0-meson photoproduction observed in e^+e^- and/or $\mu^+\mu^-$ dilepton mode. The dilepton mass spectrum was shown to have a two-component structure corresponding to the decays of ρ^0-meson inside and outside the target nucleus. The inside component can be approximately described by a Breit-Wigner formula with the in-medium modified mass and width as predicted by Eqs. (1). However, since the nucleus has a finite size, this component with a broad width does not develop a genuine pole in the complex plane of the invariant mass, M, of the lepton pair. The genuine pole in the complex M-plane pole comes only from the ρ^0-meson decays in vacuum and this outside component can be described by the standard Breit-Wigner formula with

[1] Hereafter wherever appropriate the ρ^0 will stand for the ground state $\rho^0(1S)$ meson.

the in-vacuum mass and width. Ref. [10] found that even at low energy $E \sim 2$ GeV such that $R_A/L_d \sim 2$ for heavy nuclei, the interference between the inside and outside components is substantial and produces a complex dilepton mass spectrum which cannot be described in terms of a Breit-Wigner formula with a definite mass and width. For instance, at $E = 2$ GeV the dilepton mass spectrum was found to develop a minimum near the ρ^0-meson mass. An experimental observation of this phenomenon would be of great interest. On the theoretical side, this calls for a numerical analysis within tested models of photoproduction on how a model analysis of such data would allow to distinguish the inside and outside components and extract the ρ^0-meson mass shift and collisional broadening for the inside component.

In the present paper we study the coherent reaction $\gamma^* A \to VA \to e^+e^-A, \mu^+\mu^-A$, where γ^* is a real or virtual photon and the target nucleus remains in the ground state, within the coupled-channel approach extending over the early work [10] in which the numerical calculations have been performed neglecting the off-diagonal rescatterings of ρ^0-meson. The coupled-channel analysis presented here is based on our well tested colour dipole approach (see, for instance, [17] and references therein), which was earlier successfully used in the analysis of the data on ρ^0 and J/Ψ electroproduction on nuclear targets at high energies [18, 19, 20] and vector meson production at HERA [17, 21, 22]. This analysis is of interest for two reasons. First, including the off-diagonal rescatterings allows one to check the accuracy of the one-channel approximation in the $\rho^0(1S)$-meson mass region $0.5 < M < 1$ GeV studied in ref. [10]. On the other hand, in the coupled-channel approach one can extend the mass region and investigate the medium effects for the $2S$ state $\rho'(2S)$ for which the sequential off-diagonal mechanism $\gamma^* \to \rho^0(1S) \to \rho'(2S)$ is potentially important. This extension to the $\rho'(2S)$-meson is of great interest in itself. The key feature of photoproduction of the $2S$ vector mesons on a free nucleon is strong suppression due to the nodal structure of the wave function of the $2S$ state [23, 18]. In ref. [24] it was shown that the node effect can lead to an anomalous A- and Q^2-dependence of $\rho'(2S)$ photo- and electroproduction. This effect may help to resolve the long standing problem of the D-wave vs. $2S$-wave assignment for the $\rho'(1480)$ and $\rho'(1700)$ states. The strong suppression of the cross section for the $\rho'(2S)$-meson as compared to the $\rho^0(1S)$-meson makes the experimental study of this phenomenon a challenging task. In particular, the mass spectra of the final particles in the $\rho'(2S)$ mass region can be affected by the interference with the $\rho^0(1S)$-meson Breit-Wigner tail. Our colour dipole coupled-channel approach describes very well the suppression of Ψ' production as compared with J/Ψ observed by the NMC [25, 26], E687 [27] collaborations and H1 collaboration [28] and provides a sound framework for understanding the the prospect of experimental study of the $\rho'(2S)$-meson production $\gamma^* A \to \rho^0(1S)A, \rho'(2S)A \to e^+e^-A$. In the reported numerical analysis we focus on the range of energies of the forthcoming high-luminosity experiments at TJNAF .

The paper is organized as follows. In section 2 we give the basic formulas of the coupled channel approach to the coherent $\gamma^* A \to e^+e^-A, \mu^+\mu^-A$ reaction. In section 3 we discuss evaluation of the diffraction scattering matrix. The numerical results on nuclear modifications of the in-nucleus decay component of the dilepton mass spectrum are presented in section 4.. The results are summarized in section 5.

2 The coupled channel formalism

The coupled-channel formalism for the $\gamma A \to e^+e^-A$ reaction is found in ref. [10], see also our early work [29]. For this reason, here we discuss it briefly and give only the basic formulas which are necessary for understanding technical aspects of our approach.

The standard Glauber-Gribov multiple-scattering theory [15, 16] for coherent interaction of the projectile of energy E with a nucleus is equivalent to solving the set of coupled-channel eikonal wave equations [11]:

$$\left[-\frac{\partial^2}{\partial z^2} + \hat{m}^2 + \hat{U}(\mathbf{r})\right]_{ij} \Psi_j(\mathbf{r}) = E^2 \Psi_i(\mathbf{r})\,. \tag{3}$$

Here the z-axes is chosen along the photon momentum; Ψ_i is the wave function for the channel $|i\rangle$ which can be a hadronic resonance or the initial photon; $\hat{m}^2$ is the diagonal mass operator with eigenvalues $m_i^2 = (m_i^2 - im_i\Gamma_i)\delta_{ij}$, where m_i and Γ_i are the in-vacuum mass and width of the state $|i\rangle$;, for the incident photon $\Gamma_{\gamma^*} = 0$ and $m^2_{\gamma^*} = -Q^2$ where Q^2 is the photon virtuality and the optical potential $\hat{U}(\mathbf{r})$ in (3) equals

$$U_{ij}(\mathbf{r}) = -4\pi\langle i|\hat{f}|j\rangle n_A(\mathbf{r})\,, \tag{4}$$

where $n_A(\mathbf{r})$ is the nuclear number density and $\hat{f}$ is the forward scattering matrix in the normalization

$$\mathrm{Im}\langle i|\hat{f}|i\rangle = \frac{p_i}{4\pi}\sigma_{tot}(iN \to iN)\,.$$

The boundary condition on the front face of the nucleus, $z = -R_A$, is $|i\rangle = \delta_{i\gamma^*}$.

The probability amplitude for the coherent transition $\gamma^*A \to e^+e^-A$ be written in terms of the solution $\Psi_i(\mathbf{r})$ of eq. (3) as [10]

$$T(E, M, \mathbf{p}_\perp) = N\sum_{i=h}\langle e^+e^-|t|i\rangle \int d^2\mathbf{b}dz \exp[-i(p_z z + \mathbf{p}_\perp \mathbf{b})]\Psi_i(\mathbf{r})\,, \tag{5}$$

where $\mathbf{r} = (\mathbf{b}, z)$, M is the invariant mass of the e^+e^- pair, p_z and $\mathbf{p}_\perp$ are its longitudinal and transverse momenta, respectively, $\langle e^+e^-|t|i\rangle$ is the probability amplitude for $i \to e^+e^-$ transition, N is a normalization factor which is immaterial from the point of view of the shape of the e^+e^- mass spectrum. The summation in (5) goes only over the hadronic states, which in our case are vector mesons $\rho^0(1S), \rho'(2S)$ etc. For a heavy nucleus with a mass number $A \gg 1$ and at $E \gg M$ the nuclear recoil can be neglected and the longitudinal momentum of the e^+e^- pair equals

$$p_z \approx E - \frac{Q^2 + M^2 + \mathbf{p}_\perp^2}{2E}\,. \tag{6}$$

In the coherent production $\mathbf{p}_\perp^2 \lesssim 1/R_A^2$ and in what follows we focus on $\mathbf{p}_\perp = 0$ and suppress this argument. Then by virtue of (6) the p_z-dependence of the spatial integral in the right hand side of Eq. (5) transforms directly into the M-dependence of the amplitude $T(E, M, \mathbf{p}_\perp)$ and nuclear modification of the e^+e^- spectrum.

At high energies the solution of (3) for the hadronic sector which we need for evaluation of the amplitude (5) can be written in the form

$$\Psi_h(\mathbf{b},z) = \langle h|\hat{S}(\mathbf{b},z)|\gamma^*\rangle \exp(ip_{\gamma^*}z)\,, \tag{7}$$

where the operator $\hat{S}$ is given by

$$\hat{S}(\mathbf{b},z) = \hat{P}_z \exp\left\{-\frac{i}{2p_{\gamma^*}}\int\limits_{-\infty}^{z} d\xi\left[\hat{m}^2 + Q^2 + \hat{U}(\mathbf{b},\xi)\right]\right\}. \tag{8}$$

Here, $\hat{P}_z$ is z-ordering operator, and p_{γ^*} is the photon momentum. For the numerical calculations it is convenient to treat in Eq. (8) the off-diagonal part of the optical potential in the hadronic sector as a perturbation while the diagonal transitions are included to all orders. Then, following Ref. [29], one can represent the matrix elements of the operator $\hat{S}(\mathbf{b},z)$ in the form of the ν-fold off-diagonal rescatterings series

$$\langle h|\hat{S}(\mathbf{b},z)|\gamma^*\rangle = \sum_{\nu=0}^{\infty}\langle h|\hat{S}^{(\nu)}(\mathbf{b},z)|\gamma^*\rangle\,, \tag{9}$$

where

$$\langle h|\hat{S}^{(0)}(\mathbf{b},z)|\gamma^*\rangle = -\frac{1}{2}\sigma_{h\gamma^*}\int\limits_{-\infty}^{z} dz_1 n_A(\mathbf{b},z_1)\exp[ik_{\gamma^*h}(z-z_1) - \frac{1}{2}t(\mathbf{b},z,z_1)\sigma_{hh}]\,, \tag{10}$$

$$\begin{aligned}\langle h|\hat{S}^{(\nu)}(\mathbf{b},z)|\gamma^*\rangle = \left(-\frac{1}{2}\right)^{\nu+1}&\sum_{i_1,\ldots i_\nu}\sigma^{'}_{hi_\nu}\sigma^{'}_{i_\nu i_{\nu-1}}\cdots\sigma_{i_1\gamma^*}\exp(ik_{\gamma^*h}z)\\ &\times\int\limits_{-\infty}^{z} dz_{\nu+1}n_A(\mathbf{b},z_{\nu+1})\exp[ik_{hi_\nu}z_{\nu+1} - \frac{1}{2}t(\mathbf{b},z,z_{\nu+1})\sigma_{hh}]\\ &\times\int\limits_{-\infty}^{z_{\nu+1}} dz_\nu n_A(\mathbf{b},z_\nu)\exp[ik_{i_\nu i_{\nu-1}}z_\nu - \frac{1}{2}t(\mathbf{b},z_{\nu+1},z_\nu)\sigma_{i_\nu i_\nu}]\cdots\\ \times\int\limits_{-\infty}^{z_2} dz_1 n_A(\mathbf{b},z_1)\exp[ik_{i_1\gamma^*}z_1 - &\frac{1}{2}t(\mathbf{b},z_2,z_1)\sigma_{i_1i_1}]\,,\qquad \nu\geq 1\,.\end{aligned} \tag{11}$$

Here, $\sigma^{'}_{ik} = \sigma_{ik} - \delta_{ik}\sigma_{ii}$, the matrix $\hat{\sigma}$ is connected with the forward diffraction scattering matrix

$$\hat{f} = \frac{ip_{\gamma^*}}{4\pi}\hat{\sigma}\,, \tag{12}$$

$$t(\mathbf{b},z_2,z_1) = \int_{z_1}^{z_2} dz n_A(\mathbf{b},z) \tag{13}$$

is the partial optical thickness, and

$$k_{ij} = \frac{m_i^2 - im_i\Gamma_i - m_j^2 + im_j\Gamma_j}{2E}\,, \tag{14}$$

$$k_{h\gamma^*} = -k_{\gamma^*h} = \frac{m_i^2 - im_i\Gamma_i + Q^2}{2E}\,. \tag{15}$$

The exponential factor $\exp[ik_{\gamma^* h}(z-z_1) - \frac{1}{2}t(\mathbf{b},z,z_1)\sigma_{ii}]$ in (10), (11) sums elastic, diagonal, iN rescatterings to all orders.

The real part of (15) - the longitudinal momentum transfer in $j \to i$ transition - rises with the difference between m_i and m_j. Consequently, the oscillating exponential factors in (10), (11)) lead to the form factor suppression of the contribution from heavy intermediate resonance states and the related form factor suppression of heavy mass production and of the coherent cross section at large Q^2, when the longitudinal momentum transfer $k_{h\gamma^*}$ in the $\gamma^* \to h$ transition becomes large. Precisely the same form factor effect generates strong dependence of the probability amplitude (5) on the mass of the e^+e^- pair so that the shape of resonances would differ strongly from the standard Breit-Wigner one.

Eq. (5) quantifies the separation of the production amplitude $T(E,M)$ into the inside and outside components. Namely, beyond the target nucleus the z-dependence of wave functions $\Psi_i(z,\mathbf{b})$ follows the in-vacuum decay law and the corresponding outside contribution to $T(E,M)$ has the familiar form of the sum of Breit-Wigner amplitudes with residues proportional to $\Psi_i(z=+R_A,\mathbf{b})$. The nuclear effects cam modify dramatically both the relative amplitude and phase of these residues compared to $\sigma_{h\gamma^*}$ for the free nucleon case. As explained in the Introduction, the inside contribution is a Fourier transform over the finite range $-R_A < z < R_A$ and could develop the Breit-Wigner form with the shifted mass and collision-broadened width only provided that $L_d \ll R_A$.

The first order term (10) corresponds to the standard Glauber approximation when the state $|h\rangle$ produced in the $\gamma^* \to h$ transition then propagates through the nucleus without inelastic rescatterings. The correction from the off-diagonal rescatterings is given by (11) and is responsible for the color transparency phenomenon in electroproduction of vector mesons at high Q^2 where it changes drastically the cross section as compared with the Glauber model predictions. However, as will be seen from our results for $\gamma^* A \to \rho'(2S)A$ reaction the off-diagonal effects come into play already at moderate values of the photon virtuality $Q^2 \lesssim 1$ GeV^2. This is a consequence of strong suppression of the direct $\gamma^* \to \rho'(2S)$ transition. As a result, the sequential mechanism $\gamma^* \to \rho^0(1S) \to \rho'(2S)$, involving the off-diagonal $\rho^0(1S) \to \rho'(2S)$ rescattering, becomes important even at $Q^2 = 0$.

3 Calculation of the forward diffraction matrix

As an input to the coupled-channel calculations one needs the forward diffraction matrix. At high energies it can be written as a sum of the Pomeron and reggeon contributions

$$\hat{\sigma} = \hat{\sigma}_{I\!P} + \hat{\sigma}_R \,. \tag{16}$$

At energies $E \gtrsim 2$ GeV to be considered in our paper, the dominating contribution to the $\hat{\sigma}$ comes from the Pomeron exchange. We evaluate the Pomeron exchange within the dipole approach describing the resonances as nonrelativistic $q\bar{q}$ states. Then the Pomeron contribution to the diffraction matrix element σ_{ij} for hadronic states can be written as

$$\langle i|\hat{\sigma}_{I\!P}|k\rangle = \int d^2\boldsymbol{\rho} dz \psi_i^*(\boldsymbol{\rho},z)\sigma(\rho)\psi_k(\boldsymbol{\rho},z)\,, \tag{17}$$

where $\boldsymbol{\rho}$ is the transverse size of the $q\bar{q}$ pair, $\psi_{i,k}(\boldsymbol{\rho},z)$ are the wave functions describing the $q\bar{q}$ states, and $\sigma(\rho)$ is the cross section of interaction of the $q\bar{q}$ pair with a nucleon.

We also need the excitation matrix elements $\langle i|\hat{\sigma}|\gamma^*\rangle$ for the $\gamma^* \to q\bar{q}$ excitation on a free nucleon which in the non-relativistic approximation proceed into $q\bar{q}$ states with the sum of quark helicities equal to the photon helicity [23]. Using the corresponding perturbative light-cone wave function of the virtual photon [30], we have [23]

$$\langle i|\hat{\sigma}|\gamma^*\rangle = C\int d^2\boldsymbol{\rho}\psi_i^*(\boldsymbol{\rho}, z=0)\sigma(\rho)K_0(\epsilon\rho)\,, \tag{18}$$

where

$$\epsilon^2 = m_q^2 + Q^2/4\,, \tag{19}$$

m_q is the quark mass, $K_0(x)$ is the modified Bessel function. In the present paper we focus on the nuclear-modification of the shape of resonances, and the absolute value of the normalization factor C in Eq. (18), and in Eq. (5) as well, is immaterial.

We use the oscillator wave functions for the $q\bar{q}$ states, which simplifies considerably the numerical calculations: because of azimuthal symmetry of $\sigma_{I\!P}(\rho)$ only the off-diagonal rescatterings change only the transverse excitations with zero azimuthal quantum number can be excited in the intermediate state. Excitation energy of the transverse $q\bar{q}$ oscillator equals $2\hbar\omega$, here ω is the oscillator frequency. We take in our analysis the quark mass $m_q = m_\rho/2$ and the oscillator frequency $\omega = (m_{\rho'} - m_{\rho^0})/2 \approx 0.35$ GeV , assuming 1480 MeV for the mass of the radial excitation of ρ^0-meson. For the widths of the first two excitations we use the values $\Gamma_{\rho^0} \approx 150$ MeV and $\Gamma_{\rho'} \approx 285$ MeV and, following the string model [31], assume $\Gamma_i \propto m_i$ for higher lying states. We are not sensitive to this latter assumption, though, because the contribution of the higher excitations turns out to be very small.

The experimental data on the low-x structure function F_2 and vector meson electroproduction off nucleon can be described by representing $\sigma(\rho)$ as a sum of the energy dependent perturbative and energy independent nonperturbative components [17, 22, 32]. Here we focus on the energy region $E \lesssim 20$ GeV where the energy dependence of the dipole cross section can be neglected to first approximation. Also, in the present analysis we are sensitive to $\sigma(\rho)$ mostly in the nonperturbative region of $\rho \gtrsim 0.5$. Here the gross features of $\sigma(\rho)$ are well parameterized by the two-gluon exchange model of the Pomeron [33, 34]:

$$\sigma(\rho) = \frac{16\alpha_S^2}{3}\int d^2\mathbf{q}\,\frac{[1-\exp(i\mathbf{q}\boldsymbol{\rho})][1-G_2(\mathbf{q},-\mathbf{q})]}{(\mathbf{q}^2+\mu_g^2)^2}\,, \tag{20}$$

here $G_2(\mathbf{q}_1,\mathbf{q}_2) = \langle N|\exp(i\mathbf{q}_1\mathbf{r}_1 + i\mathbf{q}_2\mathbf{r}_2)|N\rangle$ is the two-quark form factor of the nucleon, $\mu_g 0.3$ GeV is an infrared cutoff. It reproduces the colour transparency property $\sigma(\rho) \propto \rho^2$ at small ρ, by which the point-like $q\bar{q}$ system, which can be represented as a superposition of an infinite set of the resonance states, propagates through the nucleus without interaction. This color transparency phenomenon in terms of the resonance states is connected with exact cancellation of the diagonal and off-diagonal amplitudes [35]. The coupling constant α_S was normalized so the Pomeron contribution to the $\rho^0 N$ total cross section $\sigma_{I\!P}^{tot}(\rho^0 N) = \langle\rho^0|\hat{\sigma}_{I\!P}|\rho^0\rangle \approx 20$ mb. In this case the two-gluon formula gives at $\rho \gtrsim 0.5$ fm the $\sigma(\rho)$ which is close to the dipole cross section extracted from the analysis of the experimental data on electroproduction of vector mesons [17]. Hereafter we shall consider

real, $Q^2 = 0$, and virtual, $Q^2 = 1$ GeV^2, photoproduction. With our nonrelativistic wave functions we find

$$R(2S/1S) = \frac{\langle \rho'(2S)|\hat{\sigma}|\gamma^*\rangle}{\langle \rho^0(1S)|\hat{\sigma}|\gamma^*\rangle} = \begin{cases} 0.21, & Q^2 = 0, \\ 0.5, & Q^2 = 1 \text{ GeV}^2, \end{cases} \tag{21}$$

which is close to predictions of ref. [17] obtained for the relativized wave functions. At $\rho \lesssim 0.5$ fm the present parameterization gives $\sigma(\rho)$ somewhat larger than that of ref. [17]. However, because of the larger quark mass in the present nonrelativistic model for $q\bar{q}$ states the resulting diffractive matrix turn out to be close to that of ref. [17]. At this point, it must be made clear that the two-gluon parameterization (20) of $\sigma(\rho)$ is oriented towards description of the combined nonperturbative+perturbative dipole cross section and μ_g is a phenomenological parameter which must not be taken at the face value. The analysis [32] of low-x HERA data on the proton structure function F_{2p} within the generalized BFKL equation [36], and the nonperturbative evaluation of the gluon correlation radius [37] yield a clearcut evidence in favor of the infrared cutoff $\mu_G \sim 0.75$ GeV for the perturbative dipole cross section.

In our calculations we take into account the first 4 transverse excitations. The Pomeron contribution to the diffraction matrix in terms of these transverse oscillator states which we obtained from Eq. (17) for our parameterization (20) of $\sigma(\rho)$ is given by

$$\langle i|\hat{\sigma}_{\mathbb{P}}|k\rangle \approx \begin{pmatrix} 20 & -10.1 & -4.8 & 2.4 \\ -10.1 & 30.2 & -8.0 & 5.2 \\ -4.8 & -8.0 & 32.9 & 6.5 \\ 2.4 & 5.2 & 6.5 & 34.1 \end{pmatrix}_{ik} . \tag{22}$$

Here the matrix elements in (22) are in units of mb, i and k are the radial quantum numbers of the transverse oscillators (as was said above the Pomeron exchange does not change the longitudinal quantum number). The matrix (22) shows clearly the decrease of the off-diagonal amplitudes with increase of the difference between the initial and final radial quantum numbers $|i - k|$ which derives from the oscillation of the resonance wave function and, in conjunction with the form factor effect, suppresses the contribution of higher excitations in the production amplitude matrix element (11). Using the three-dimensional $\rho'(2S)$-meson wave function from (22) one obtains for the Pomeron contribution to the $\rho'(2S)N$ total cross section $\sigma^{tot}_{\mathbb{P}}(\rho'(2S)N) = \langle \rho'(2S)|\hat{\sigma}_{\mathbb{P}}|\rho'(2S)\rangle \approx 27$ mb.

In parameterizing the reggeon contribution to the diffraction matrix we assume that the secondary reggeon exchanges can be treated in terms of scattering amplitudes for the quark (or antiquark) making up the $q\bar{q}$ state as predicted by the dual parton model [38] and quark gluon string model [39] based on the idea of the topological expansion [40]. In this case one can neglect the reggeon contribution to the off-diagonal transitions, and for all excited ρ' states the reggeon contribution to diagonal $\rho' N$ scattering amplitudes turn out to be equal to the reggeon contribution to the $\rho^0(1S)N$ scattering amplitude. This amplitude is dominated by the contribution of the Regge pole P' which can be written in the Regge approach as

$$\langle \rho^0|\hat{\sigma}_R|\rho^0\rangle = \boldsymbol{\rho}_{P'} \left(\frac{s}{s_0}\right)^{\alpha_{P'}-1} \left[1 + i\frac{1 + \cos \pi\alpha_{P'}}{\sin \pi\alpha_{P'}}\right] , \tag{23}$$

where $s = m_N^2 + 2Em_N$. In our analysis we take the standard reggeon intercept $\alpha_{P'} = 0.5$. The residue $r_{P'}$ has been adjusted to reproduce at $E \sim 10$ GeV the real part of the $\rho^0 N$ scattering amplitude extracted in ref. [12] from the experimental data for ρ^0-meson photoproduction using the vector dominance model. For $s_0 = 1$ GeV^2 this gives $r_{P'} \approx 15$ mb. The nonzero Re/Im ratio for the diffraction scattering matrix leads to the mass shift for the resonance states decaying inside the nucleus. For the ρ^0-meson in the energy region $E \sim 2 - 20$ GeV considered in the present paper it gives $\Delta m_{\rho^0} \sim$ 50-100 MeV.

For evaluating the e^+e^- mass spectrum we need also the transition amplitude $\langle e^+e^-|t|i\rangle$ which enters Eq. (5). Following the authors of ref. [10] we neglect a possible smooth M-dependence of this transition amplitude as compared with that coming from the spatial integral in the right hand side of (5), and take $\langle e^+e^-|t|i\rangle \propto \psi_i(\mathbf{r} = 0)$ as predicted by the nonrelativistic model of $q\bar{q}$ states. Note that in the nonrelativistic approach the D-wave $q\bar{q}$ state does not contribute to the di-lepton production. For this reason, the absence of splitting the $2S$- and D-states in the oscillator model is not very important from the point of view of the e^+e^- mass spectrum.

The applicability of the full fledged couple-channel formalism depends on the two space-time scales: the formation length L_f, associated with the $i \to k$ transitions,

$$L_f = \frac{1}{k_{ik}} = \frac{2E}{m_i^2 - m_k^2} \sim \frac{2E}{m_{\rho'}^2 - m_{\rho^0}^2} \approx 0.25fm \cdot \frac{E}{1\text{GeV}}\,, \tag{24}$$

and the coherence length

$$L_c = \frac{1}{k_{h\gamma^*}} = \frac{2E}{M^2 + Q^2} \approx 0.75fm \frac{E}{1\text{GeV}} \cdot \frac{m_{\rho^0}^2}{M^2 + Q^2} \tag{25}$$

associated with the transition $\gamma^* \to i$. Strictly speaking, evaluation of diffraction matrix from equation (17) and of excitation amplitudes from (18) in terms of the color dipole cross section only holds if $L_f > R_N$ and $L_c > R_N$. For the interesting to us region $Q^2 \lesssim 1$ GeV^2 and for the $\rho^0(1S)$- and $\rho'(2S)$-mesons the full fledged coupled-channel effects develop only at $E \sim 5-8$ GeV. However, at lower energy the only change is the decoupling of excitation of higher excitations from the photon and of off-diagonal diffractive transitions to and from higher excitations and we can stretch the formalism even down to $E = 2$ GeV. At this energy we have a single-channel problem with $\gamma^* \to \rho^0$ excitation followed by diagonal $\rho^0 N$ scattering. For the evaluation of the relevant diagonal elastic rescatterings we only need the $\rho^0 N$ total cross section and the color dipole value of $\langle \rho^0|\hat{\sigma}_{\mathbf{I\!P}}|\rho^0\rangle$ does still a good job for the almost energy independent Pomeron contribution. Simultaneously, $\langle \rho^0|\hat{\sigma}|\gamma^*\rangle$ enters only as the overall normalization and whether it is evaluated from eq. (18) or within different approach does not affect nuclear modifications of the e^+e^- mass spectrum.

4 Numerical results

4.1 The input parameters

We have performed the numerical calculations for the energies $E = 2,\ 5,\ 10, 20$ GeV at $Q^2 = 0$ and 1 GeV^2 for the target nuclei ^{9}Be, ^{56}Fe and ^{207}Pb. For the parameterization of

the diffractive matrix and of the photon and vector meson wave functions see section 3. For the nuclear matter density in the light target nucleus ^{9}Be we use the oscillator shell model with the oscillator frequency adjusted to reproduce the experimental value of the root-mean-square radius of the charge distribution $\langle r^2\rangle^{1/2}_{^9Be} = 2.51$ fm [41]. For the target nucleus ^{56}Fe the parameterization of the nuclear density by a sum of Gaussians from ref. [41] was used. For ^{207}Pb we use the Wood-Saxon parameterization of the nuclear density with parameters borrowed from [41].

4.2 The basis of vector meson states

As stated above, in our numerical calculations we include 4 transverse resonance states. For the number of the off-diagonal rescatterings of the $q\bar{q}$ state we take $\nu = 2$. We checked that in our kinematic region the contribution from higher excitations and higher order off-diagonal rescatterings can safely be neglected. Furthermore, an approximation of the first two states and one off-diagonal rescattering of the $q\bar{q}$ state is sufficient for all the practical purposes. Our principal interest is in the interplay of nuclear effects and interference of the $\rho^0(1S)$ and $\rho'(2S)$ and we did not include the numerically smaller contributions from the ω- and ϕ-mesons and their excitations. These long-lived resonances decay for the most part outside the target nucleus and the nuclear effects do not modify considerably their shapes.

4.3 The presentation of results

Due to the above mentioned form factor effect connected with the longitudinal momentum transfer and the suppression of the $\rho'(2S)$ production by the node effect the amplitude (5) decreases strongly with increase of the mass of the e^+e^- pair. In order to facilitate graphical presentation of the results, following Ref. [10] we use the scaled amplitude

$$T'(E,M) = M^2 T(E,M)/A\,. \tag{26}$$

Since in the absence of absorption effects (5) gives the amplitude $\propto A$, in (26) we also introduced the factor $1/A$. Our principal numerical results for the mass spectrum are shown in figs. 1-6 in the form of

$$|T'|^2 \propto \frac{M^4}{A^2}\frac{d\sigma}{dM^2 dp_\perp^2}\bigg|_{p_\perp=0}\,.$$

We focus on the mass range $M < 1.75$ GeV and include as final states the $\rho^0(1S)$ and $\rho'(2S)$ vector mesons.

In order to see better the resonance behaviour of production amplitudes we also show in figs. 7-9 the Argand plots for T'.

Now we shall comment on the salient features of the Q^2- , energy and nuclear target dependence of these mass spectra.

4.4 The nucleon target

The reference e^+e^- mass spectrum for the proton target and the photon energy $E = 5$ GeV is shown by thick solid curves in figs. 1b-6b. In the approximation of the energy independent dipole cross section $\sigma(\rho)$ it does not depend on the photon energy E. The mass spectrum exhibits the well separated $\rho^0(760)$ and $\rho'(1480)$ resonance peaks. Recall the factor M^4 which makes the $\rho'(2S)$ tail about flat at large M^2.

The suppression by the node effect is lifted with increasing Q^2, see eq. (21), and the comparison of the mass spectra for real, $Q^2 = 0$, and virtual, $Q^2 = 1$ GeV^2, photoproduction shows clearly the predicted rise of the $\rho'(2S)/\rho^0(1S)$ ratio with increasing Q^2 [23, 18, 24]. This rise of the $\rho'(2S)$ signal with Q^2 is clearly seen from a comparison of the Argand diagrams of fig. 7b and fig. 7b.

4.5 Mass shift *vs.* nuclear form factor effects: the ρ^0 region at low energy

In figs. 1a-6a we show the mass spectrum for low energy, $E = 2$ GeV, at which the $\rho'(2S)$ production is negligible and the single-channel Glauber approximation (10) holds. The energy $E = 2$ is very low such that the ρ^0 would be expected to decay within nucleus. Although this reasoning is correct, our results show that the effect of the mass shift (1) due to the real part of the forward $\rho^0 N$ scattering amplitude proves to be marginal in the nuclear modification of the inside component of the production amplitude. The point is that mass shift enters the exponent of the integrand in (10) via the extra phase

$$\phi = \frac{1}{2} t(\mathbf{b}, z, z_1) \mathrm{Im}\sigma_{hh} \approx \frac{1}{2} \cdot r_{\mathbb{P}'} n_A (z - z_1) \sqrt{\frac{s_0}{s}} (z - z_1) \tag{27}$$

which must be compared to the phase $k_{\gamma^* h}(z - z_1) = -(z - z_1)/L_c$ from the finite coherence length. Evidently, the significance of the mass shift for the inside component of the dilepton production amplitude is controlled by the parameter

$$\eta = \frac{1}{2} \cdot r_{\mathbb{P}'} n_A \sqrt{\frac{s_0}{s}} L_c \approx 0.1 \frac{m_\rho^2}{M^2 + Q^2} \sqrt{\frac{E}{1 \text{ GeV}}} \,. \tag{28}$$

In the numerical evaluation in (28) we used the standard parameters of the $\rho^0 N$ interaction as cited in section 3 and normal nuclear density. We see that the mass shift (1) amounts to a renormalization

$$k_{\gamma^* h} \to k_{\gamma^* h}(1 - \eta) \,. \tag{29}$$

At $E = 2$ GeV the parameter $\eta \ll 1$. On the other hand, the coherence length (25) is very short,

$$L_c(E = 2 \text{ GeV}) = 1.5 \text{ fm} \cdot \frac{m_{\rho^0}^2}{M^2 + Q^2} \,,$$

much smaller than nuclear radii for heavy nuclei and even for the light Be nucleus it is comparable to the nuclear radius. For this reason nuclear effects are dominated by the attenuation of the ρ^0 due to the diagonal $\rho^0 N \to \rho^0 N$ transitions and, most significantly, by distortions due to the nuclear form factor effects.

The results for the mass spectrum are shown in figs. 1a-6a by a solid curve. For the Be target the principal effect is the mass spectrum drops at $M \gtrsim 1$ GeV much faster than for the free nucleon target. For the heavy Pb target the form factor oscillations lead to an effective splitting of the ρ^0 peak - the mass spectrum develops a minimum at $M \sim m_{\rho^0}$. At $Q^2 = 1$ GeV^2 the coherence length becomes still smaller and the distortion of the e^+e^- mass spectrum by form factor effects become much stronger, such that the dip at the ρ^0 mass evolves already for the Be target. The corresponding Argand diagrams of figs. 8a and 9a span the mass range $0.5 < M < 1$ GeV and exhibit a structure more complex than a single resonance loop. Our findings for real photoproduction off Fe and Pb targets are similar to those obtained in ref. [10] for the target mass number $A = 50$ and $A = 200$ in the approximation of uniform nuclear density.

Notice that nowhere the splitting of the ρ^0 mass spectrum looks as a superposition of two Breit-Wigner peaks with the in-vacuum ρ^0 mass and the in-medium mass shifted by ≈ 50 MeV as cited in section 3. The weak impact of the in-medium shift (1) on the ρ^0 splitting is obvious from dashed curves in figs. 1a-6a which show the mass spectrum obtained when the mass shift (1) is neglected, i.e., putting $Re/Im = 0$. The distortions of the mass spectrum change little, as a matter of fact the splitting of the ρ^0 peak is even enhanced somewhat in conformity to the rescaling (29). Despite the slow rise of the parameter η with energy, in the range E =2-20 GeV of the interest for experiments at the Jefferson laboratory $\eta \ll 1$. Furthermore, at higher energies the contribution from the in-medium decays decreases and the overall effect of the mass shift becomes still weaker.

4.6 Higher energies: opening of the $\rho'(2S)$ channel.

The new feature of high energy photoproduction is opening of the $\rho'(2S)$ channel and coupled-channel effects. For the comparison purposes, we show by the thick solid curve in figs. 1b-6b the mass spectrum for the free nucleon target. The full coupled-channel results for nuclear targets comprise the attenuation, nuclear form factor effects, the effects of $\rho^0(1S) \leftrightarrow \rho'(2S)$ transitions including the multistep transitions and the resonance mass shift due to $Re/Im \neq 0$. The relative importance of these effects depends on the mass region, energy and the target mass number.

The importance of the off-diagonal transitions in the target nucleus can be judged from the comparison of the full coupled-channel results (thin solid curve) with those from the diagonal approximation (dotted curve) in which off-diagonal rescatterings are switched off, i.e., $\nu = 0$, and only the direct $\gamma^* \to \rho^0(1S)$ and $\gamma^* \to \rho'(2S)$ transitions followed by elastic $\rho^0 N$ and $\rho'(2S)N$ rescatterings are included. One can see that in the ρ^0-meson mass region $0.5 < M \lesssim 1$ GeV the effect of the off-diagonal rescatterings for both the values of Q^2 turns out to be small. Indeed, the direct $\gamma^* \to \rho^0(1S)$ transition is strong whereas the both transitions in the off-diagonal sequence $\gamma^* \to \rho'(2S) \to \rho^0(1S)$ are weak, see the description of diffraction matrix in section 3. Hereafter in our discussion of the off-diagonal effect we focus on the $\rho'(2S)$ contribution because the contribution of intermediate states heavier than $\rho'(2S)$-meson is still smaller.

Our results for real photoproduction, $Q^2 = 0$, in the $\rho^0(1S)$ mass region ^{56}Fe and ^{207}Pb targets are close to that of ref. [10] obtained for real photons for the nucleus mass numbers $A = 50$ and $A = 200$ in the approximation of uniform nuclear density.

At $Q^2 = 1$ GeV^2 the coherence length is short also for $E = 5$ GeV and distortions of the shape of the e^+e^- mass spectrum in the $\rho^0(1S)$-meson mass region by the nuclear form factor as described in subsection 4.5 persist for $E = 5$ GeV as well. The dominance of the form factor effects is obvious from the fact that these distortions change little from the full coupled-channel to diagonal case.

At higher masses the coupled channel effects become more important. Here the direct $\gamma^* \to \rho'(2S)$ transition is weak and there is a strong interference with the off-diagonal sequential transition $\gamma^* \to \rho^0(1S) \to \rho'(2S)$ which contains a comparably weak transition $\rho^0(1S) \to \rho'(2S)$. As a matter of fact, for heavy target nuclei the sequential mechanism $\gamma^* \to \rho^0(1S) \to \rho'(2S)$ is found to dominate over the direct mechanism $\gamma^* \to \rho'(2S)$, which can be seen as follows. In figs. 1-6 we show by the dashed and long-dashed curve the pure $\rho^0(1S)$ and the $\rho'(2S)$ contributions evaluated in the full coupled-channel approach, $\nu = 2$. The dot-dashed curve shows the pure $\rho'(2S)$ contribution evaluated in the diagonal approximation, $\nu = 0$, and in this approximation the $\rho'(2S)$ signal is much weaker than in the coupled-channel case in which the $\rho'(2S)$ is fed by sequential transitions. This is a very interesting example when the $\rho'(2S)$ production off heavy nuclei opens a possibility for extracting the matrix element $\langle\rho'(2S)|\hat{\sigma}|\rho^0(1S)\rangle$ from the experimental data on the e^+e^- mass spectrum in the $\rho'(2S)$ mass region. The measurement of this matrix element could give a unique information on the overlap of the $\rho^0(1S)$ and $\rho'(2S)$ wave functions.

The $\rho^0(1S)$-$\rho'(2S)$ interference changes from destructive at masses M below the $\rho'(2S)$ peak to constructive at, and above, the $\rho'(2S)$ peak, reflecting the mass dependence of the relative phase of the $\rho^0(1S) \to e^+e^-$ and $\rho'(2S) \to e^+e^-$ Breit-Wigner amplitudes: i) the mass spectrum develops a dip in between the $\rho^0(1S)$ and $\rho'(2S)$ resonance peaks, where the coupled-channel, thin solid, curve goes below the thin solid curve for the pure $\rho^0(1S)$ contribution, ii) at, and beyond, the $\rho'(2S)$ peak the coupled-channel, thin solid curve goes well above the long-dashed curve for the pure $\rho'(2S)$ contribution, which testifies to a substantial contribution form the large-mass tail of the $\rho^0(1S)$ in the $\rho'(2S)$ region. Evidently, that makes impossible an experimental extraction of the cross section of $\rho'(2S)$ production in a probabilistic approach when the interference with the Breit-Wigner tail of $\rho^0(1S)$-meson is neglected.

4.7 The form factor effects in the $\rho'(2S)$ region.

For moderate energies and heavier nuclei, and also for larger Q^2, we encounter the situation when the coherence length L_c for the $\rho'(2S)$ mass region becomes comparable to and/or smaller than the nuclear radius R_A. In this case the $\rho'(2S)$ signal will be subject to distortions by the form factor effect in precisely the same manner as the ρ^0 signal at lower energies, see section 4.5. For instance, in real photoproduction off ^{56}Fe target at $E = 5$ GeV the $\rho'(2S)$ peak splits into two bumps with the dip at $M \approx m_{\rho'}$, see fig. 3b. The point that this dip is connected with the form factor effects is evident from the shift of the dip towards the smaller values of M, and the development of the secondary dip, with the increase of Q^2, compare figs. 3b and 4b. The results for heavy target, ^{207}Pb, fig. 5b to fig. 5c to fig 5d show clearly how the dip-bump structure moves to higher masses M with the increase of the coherence length L_c with rising energy E.

A comparison of Argand diagrams for the free nucleon target, fig. 7, and nuclear tar-

gets, figs. 8 and 9, shows that the resonance loop corresponding to the $\rho'(2S)$-meson becomes well visible only at $E \gtrsim 10$ GeV. However, even in this energy region the contribution to the amplitude from the Breit-Wigner tail of $\rho^0(1S)$ meson cannot be neglected as compared with that from the $\rho'(2S)$ meson.

5 Conclusions

We have performed a coupled-channel analysis of nuclear-medium modification of the $\rho^0(1S)$- and $\rho'(2S)$-mesons in the coherent $\gamma^* \to \rho^0(1S)A, \rho'(2S)A \to e^+e^-A$ reaction in the kinematic region $E \sim 2-20$ GeV and $Q^2 \lesssim 1$ GeV^2. Our findings on the interplay of the inside and outside decays, in-medium modifications of the inside component and the coupled-channel effects can be summarized as follows:
(i) In the $\rho^0(1S)$ meson mass region $0.5 \lesssim M \lesssim 1$ GeV the effect of the off-diagonal rescatterings is small. For heavy nuclei in this mass region our results agree with those obtained in ref. [10] within the one-channel approximation.
(ii) The off-diagonal rescatterings become important at $M \gtrsim 1$ GeV. The main off-diagonal contribution is the $\rho'(2S)$ production through the sequential mechanism $\gamma^* \to \rho^0(1S) \to \rho'(2S)$. This mechanism dominates the cross section of $\rho'(2S)$ production for heavy nuclei.
(iii) At low energies $E \lesssim 5$ GeV the shapes of the $\rho^0(1S)$ and $\rho'(2S)$ resonances are strongly affected by the nuclear effects connected with the interference interplay of the resonance decays inside and outside the target nucleus and form factor effect connected with the longitudinal momentum transfer.
(iv) The $\rho'(2S)$ resonance is seen well only at $E \gtrsim 10$ GeV. Even at high energy its shape is affected by the interference with the Breit-Wigner tail of $\rho^0(1S)$-meson which must be included properly in an analysis of the experimental data on the e^+e^- mass spectrum in the $\rho'(2S)$ mass region.

In our analysis we focused on the dilepton decay mode. Evidently, very similar effects must be observed in measurements of the $\rho^0(1S)$ and $\rho'(2S)$ production through the $\pi\pi$ decay mode. The major difference from the dilepton mode would come from to the final-state interaction of the $\pi\pi$ system, which would reduce the relative contribution of the inside component as compared with that for the e^+e^- mode. For this reason a comparison of the mass spectra for these two cases would be of great interest. It is especially interesting at low energies $E \sim 2-5$ GeV for heavy nuclei when the inside component is large for the e^+e^- decay mode and will be strongly suppressed by the final-state absorption for the $\pi\pi$ mode. The comparative theoretical analysis of the coherent $\rho^0(1S)$ and $\rho'(2S)$ photo- and electroproduction for the e^+e^- and $\pi\pi$ decay modes is now in progress.

Acknowledgments

The work of BGZ was partially supported by the grants INTAS 96-0597 and DFG 436RUS17/11/99.

References

[1] V. Bernard and U.-G. Meissner, Nucl. Phys. **A489**, 647 (1988).

[2] A. Hosaka, Phys. Lett. **B244**, 363 (1990).

[3] G.E. Brown and M. Rho, Phys. Rev. Lett. **66**, 2720 (1991).

[4] T. Hatsuda and S.H. Lee, Phys. Rev. **C46**, R34 (1992).

[5] M. Asakawa, C.M. Ko, P. Levai and X.J. Qiu, Phys. Rev. **C46**, R1159 (1992).

[6] Y. Koike, Phys. Rev. **C51**, 1488 (1995).

[7] T. Hatsuda, S.H. Lee and H. Shiomi, Phys. Rev. **C52**, 3364 (1995).

[8] V.I. Eletsky and B.L. Ioffe, Phys. Rev. Lett. **78**, 1010 (1997).

[9] V.I. Eletsky, B.L. Ioffe and J.I. Kapusta, Eur. Phys. J. **A3**, 381 (1998); hep-ph/9907411.

[10] K.G. Boreskov, L.A. Kondratyuk, M.I. Krivoruchenko and J.H. Koch, Nucl. Phys. **A619**, 295 (1997).

[11] Ye.S. Golubeva, L.A. Kondratyuk and W. Cassing, Nucl. Phys. **A625**, 832 (1997).

[12] L.A. Kondratyuk, A. Sibirtsev, W. Cassing, Ye.S. Golubeva and M. Effenberger, Phys. Rev. **C58**, 1078 (1998).

[13] L.A.Kondratyuk, M.I.Krivoruchenko, N.Bianchi, E. De Sanctis and V.Muccifora, *Nucl. Phys.* **A579**, 453 (1994)

[14] D.V.Bugg, *Nucl. Phys.* **B88**, 381 (1975)

[15] R.J. Glauber, in: *Lectures in Theoretical Physics*, v.1, ed. W. Brittain and L.G. Dunham. Interscience Publ., N.Y., 1959; R.J. Glauber and G. Matthiae, Nucl. Phys. **B21** (1970) 135.

[16] V.N. Gribov, Sov. Phys. JETP **29** (1969) 483; **30** (1970) 709.

[17] J. Nemchick, N.N. Nikolaev, E. Predazzi and B.G. Zakharov, Z. Phys. **C75**, 71 (1997).

[18] O. Benhar, B.Z. Kopeliovich, C. Mariotti, N.N. Nikolaev and B.G. Zakharov, Phys. Rev. Lett. **69**, 1156 (1992).

[19] B.Z. Kopeliovich, J. Nemchick, N.N. Nikolaev and B.G. Zakharov, Phys. Lett. **B309**, 179 (1993).

[20] B.Z. Kopeliovich, J. Nemchick, N.N. Nikolaev and B.G. Zakharov, Phys. Lett. **B324**, 469 (1994).

[21] J. Nemchick, N.N. Nikolaev, E. Predazzi and B.G. Zakharov, Phys. Lett. **B374**, 199 (1996).

[22] J. Nemchick, N.N. Nikolaev, E. Predazzi, B.G. Zakharov and V.R. Zoller, JETP **86**, 1054 (1998).

[23] B.Z. Kopeliovich and B.G. Zakharov, *Phys. Rev.* **D44**, 3466 (1991).

[24] J. Nemchick, N.N. Nikolaev and B.G. Zakharov, Phys. Lett. **B339**, 194 (1994).

[25] NMC Collaboration: M. Arneodo, A. Arvidson, B. Badelek *et al*, Phys. Lett. **B332**, 195 (1994).

[26] NMC Collaboration: P. Amaudruz, M. Arneodo, A. Ervidson et al., Nucl. Phys. **B371**, 553 (1992).

[27] E687 Collaboration: P.L. Frabetti, H.W.K. Cheung, I.P. Cumalat et al., Report at the Europhysics Conference on High Energy Physics, Brussels, June 1995.

[28] H1 Collaboration: C. Adloff et al., *Phys. Lett.* **B421** (1998) 385.

[29] O. Benhar, S. Fantoni, N.N. Nikolaev and B.G. Zakharov, JETP **111**, 769 (1997).

[30] N.N. Nikolaev and B.G. Zakharov, Z. Phys. **C49**, 607 (1991).

[31] A. Casher, H. Neuberger and S. Nussinov, Phys. Rev. **D20**, 179 (1979).

[32] N.N. Nikolaev and B.G. Zakharov, Phys. Lett. **B327**, 149 (1994).

[33] F.E. Low, Phys. Rev. **D12**, 163 (1975).

[34] J.F. Gunion and D.E. Soper, Phys. Rev. **D15** 2617 (1977).

[35] N.N. Nikolaev, Comments Nucl. Part. Phys. **21**, 41 (1992).

[36] N.N. Nikolaev, V.R. Zoller and B.G.Zakharov, Phys. Lett. **B328**, 143 (1994).

[37] E. Schuryak, Rev. Mod. Phys. **65**, 1 (1993).

[38] A. Capella, U. Sukhatme, C.-I, Tan and J. Tran Thanh Van, Phys. Lett. **B81**, 68 (1979); Phys. Rep. **236**, 225 (1994).

[39] A.B. Kaidalov, Phys. Lett. **B116**, 459 (1982).

[40] G. Veneziano, Phys. Lett. **B52**, 220 (1974); Nucl. Phys. **B74**, 365 (1974); **B117**, 519 (1976).

[41] H. de Vries, C.W. de Jaeger and C. de Vries, Atomic Data and Nuclear Data Tables **36** 496 (1987).

Figure captions:

Fig. 1 - The $e^+e^-, \mu^+\mu^-$ rescaled mass spectrum (in arbitrary units) for coherent real photoproduction, $Q^2 = 0$, off the ^{9}Be nucleus for the incident beam energy $E = 2, 5, 10$ and 20 GeV. The legend of curves in box *(a)*: The solid curve is a prediction of the Glauber approximation with mass shift (10) from the reggeon amplitude (23) included, the dashed line shows the results obtained neglecting the mass shift. The legend of curves in box *(b)*: The thick solid curve is the spectrum for the nucleon target, all other curves are for nuclear target. The thin solid curve is the full coupled-channel calculation, $\nu = 2$ in expansion (10). The dotted curve is a result from the diagonal approximation, $\nu = 0$ in expansion (10), the $\rho^0(1S)$-$\rho'(2S)$ interference in the e^+e^- and/or $\mu^+\mu^-$ decay channels included. The dashed curve shows the pure ρ^0 signal in the coupled-channel calculation, $\nu = 2$. The long-dashed curve is the $\rho'(2S)$ signal in the coupled-channel calculation, $\nu = 2$. The dot-dashed curve is the $\rho'(2S)$ signal in the diagonal approximation, $\nu = 2$. Boxes *(c)* and *(d)* are the same as box *(b)* but for $E = 10$ and 20 GeV, respectively, and with omission of mass spectrum for the free nucleon target.

Fig. 2 - The same as Fig. 1 but for virtual photoproduction, $Q^2 = 1$ GeV^2.

Fig. 3 - The same as Fig. 1 but for the target nucleus ^{56}Fe.

Fig. 4 - The same as Fig. 2 but for the target nucleus ^{56}Fe.

Fig. 5 - The same as Fig. 1 but for the target nucleus ^{207}Pb.

Fig. 6 - The same as Fig. 2 but for the target nucleus ^{207}Pb.

Fig. 7 - The Argand plots for the scaled amplitude $T' = M^2T(E, M)$ for *(a)* real, $Q^2 = 0$, and *(b)* virtual, $Q^2 = 1$ GeV^2, photoproduction off the free nucleon target.

Fig. 8 - - The Argand plots for the scaled amplitude (26) at $Q^2 = 0$. The solid, dotted, and dashed curves show the results for the target nucleus ^{207}Pb, ^{56}Fe, and ^{9}Be, respectively. The curves are given in arbitrary units. The mass intervals are 0.5-1 GeV for $E = 2$ GeV, and 0.5-2 GeV for $E = 5$, 10, and 20 GeV. The spacing of mass points along the curves is 0.25 GeV, the arrows show the direction of the increasing mass.

Fig. 9 - The same as Fig. 8 but for $Q^2 = 1$ GeV^2.

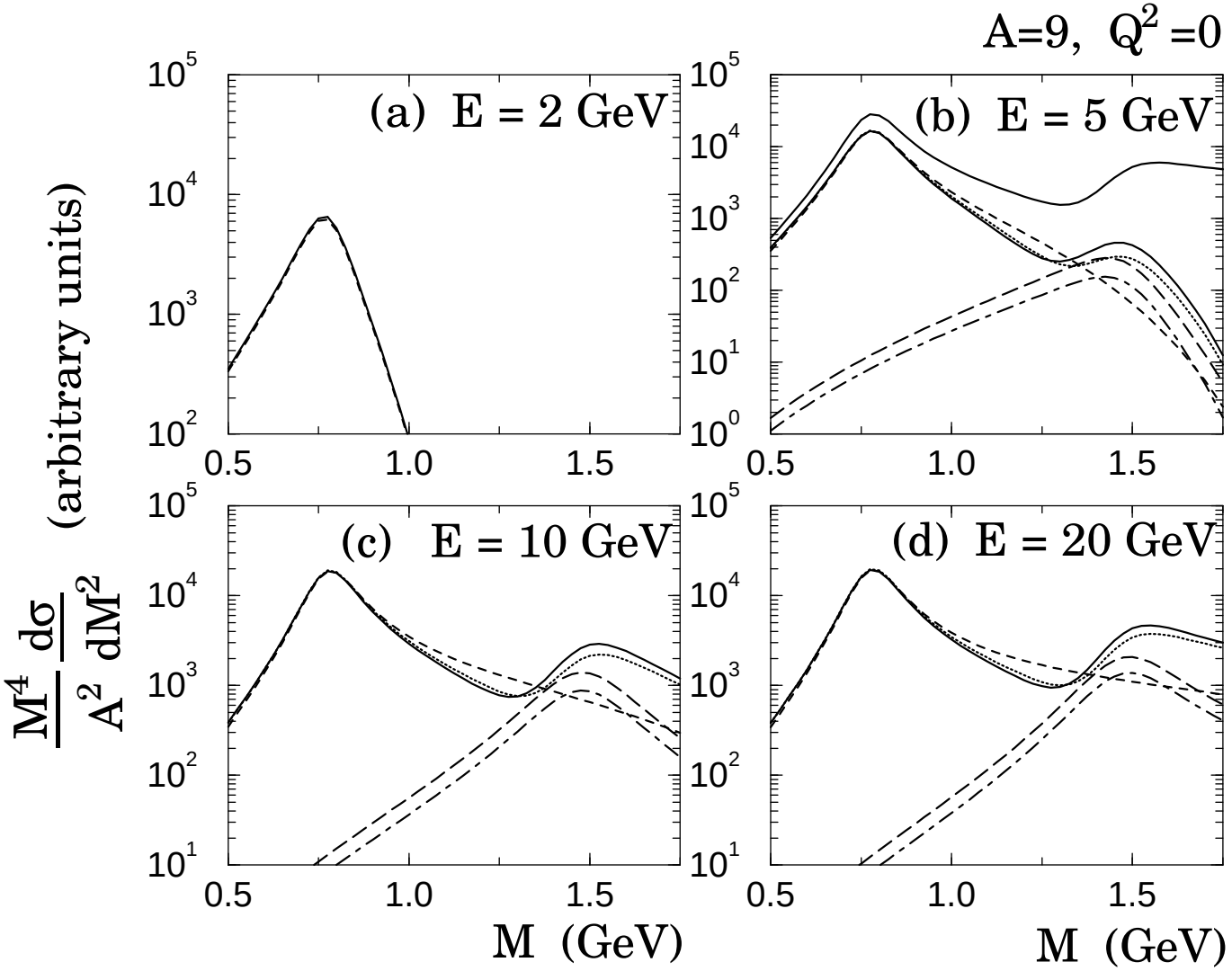
A=9, Q^2 =0
(a) E = 2 GeV
(b) E = 5 GeV
(c) E = 10 GeV
(d) E = 20 GeV
$\frac{M^4}{A^2}\frac{d\sigma}{dM^2}$ (arbitrary units)
M (GeV)
M (GeV)

Fig.1

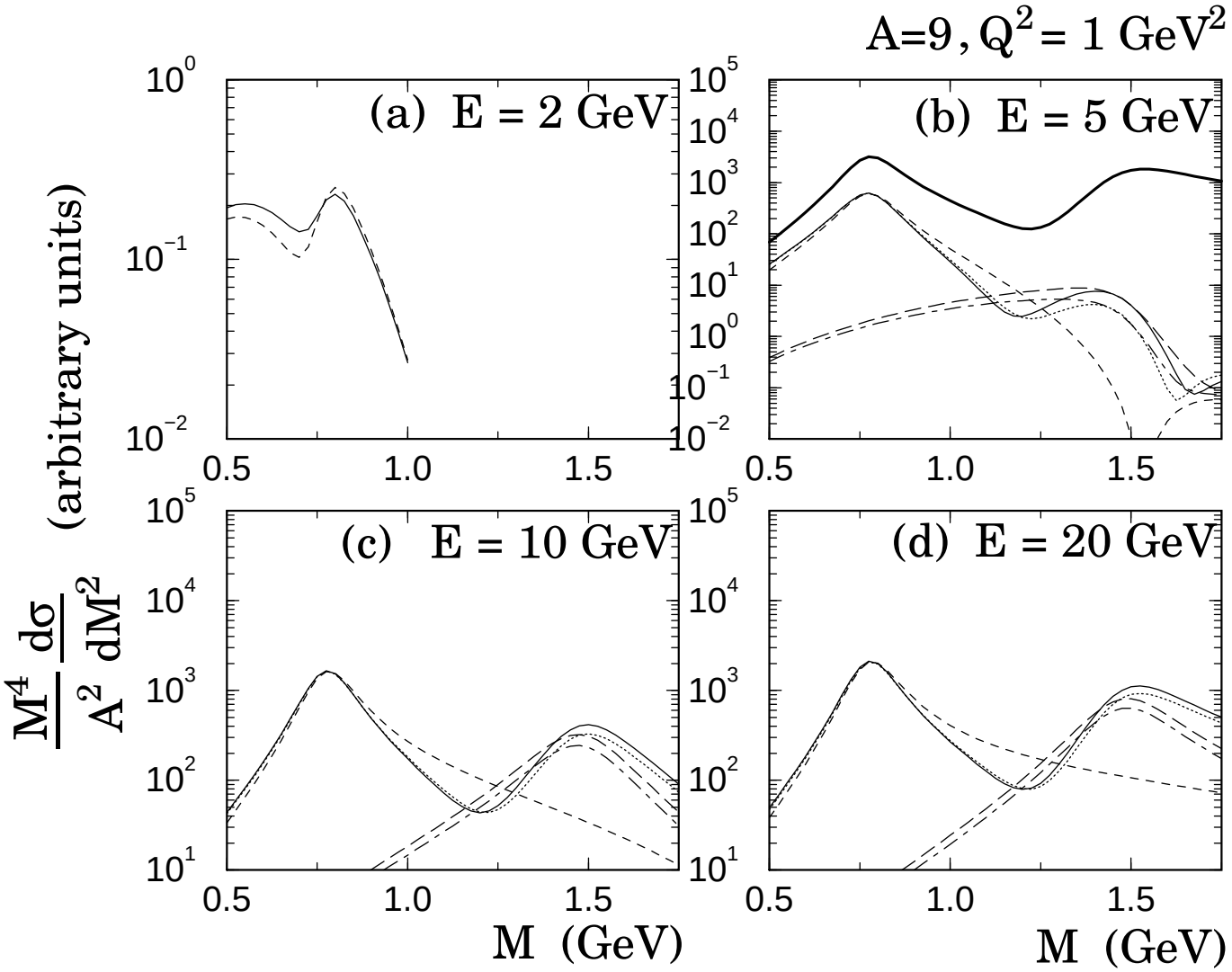
A=9, Q^2= 1 GeV^2
(a) E = 2 GeV
(b) E = 5 GeV
(c) E = 10 GeV
(d) E = 20 GeV
$\frac{M^4}{A^2}\frac{d\sigma}{dM^2}$ (arbitrary units)
M (GeV)
M (GeV)

Fig. 2

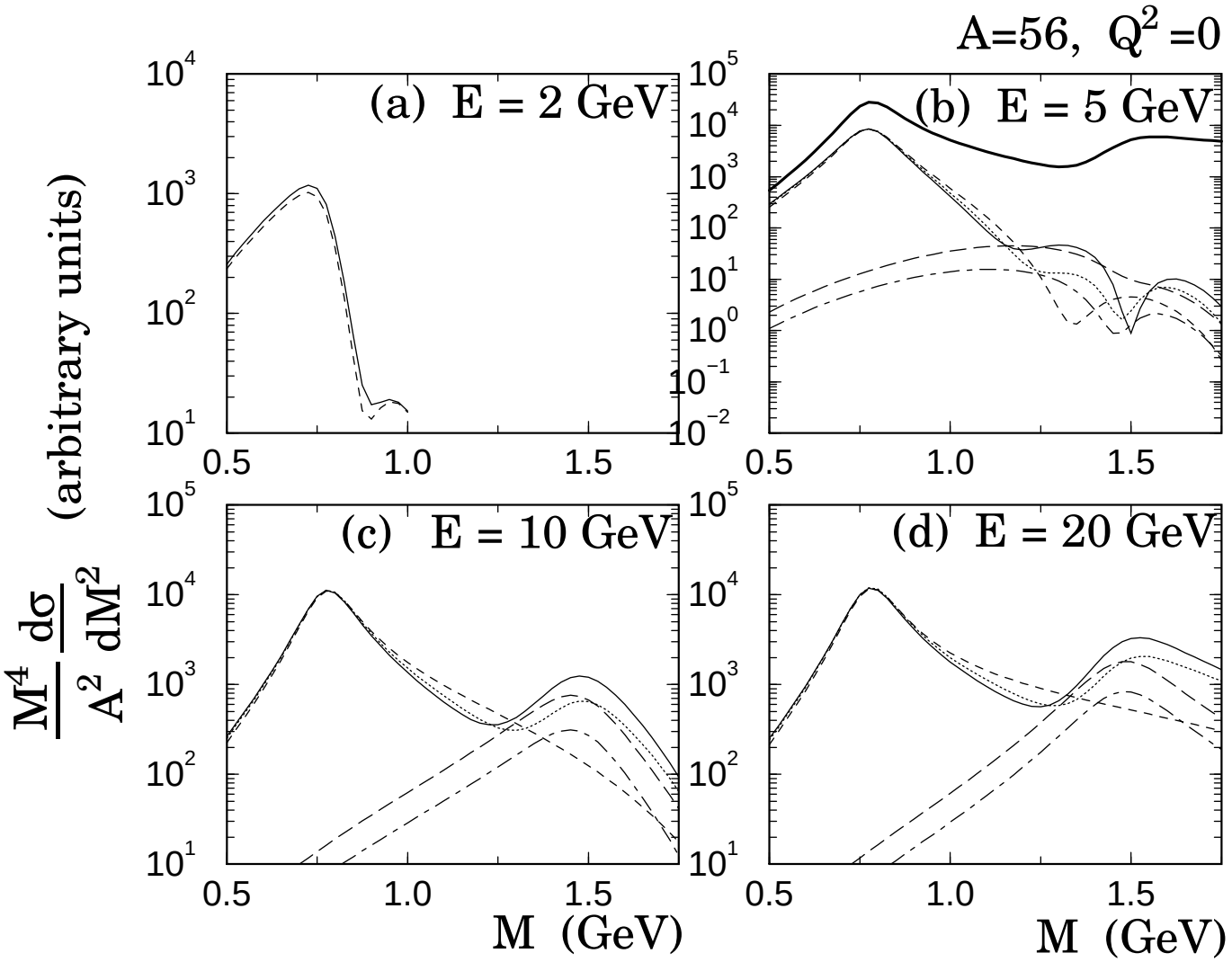
A=56, Q^2 =0
(a) E = 2 GeV
(b) E = 5 GeV
(c) E = 10 GeV
(d) E = 20 GeV
$\frac{M^4}{A^2}\frac{d\sigma}{dM^2}$ (arbitrary units)
M (GeV)
M (GeV)

Fig. 3

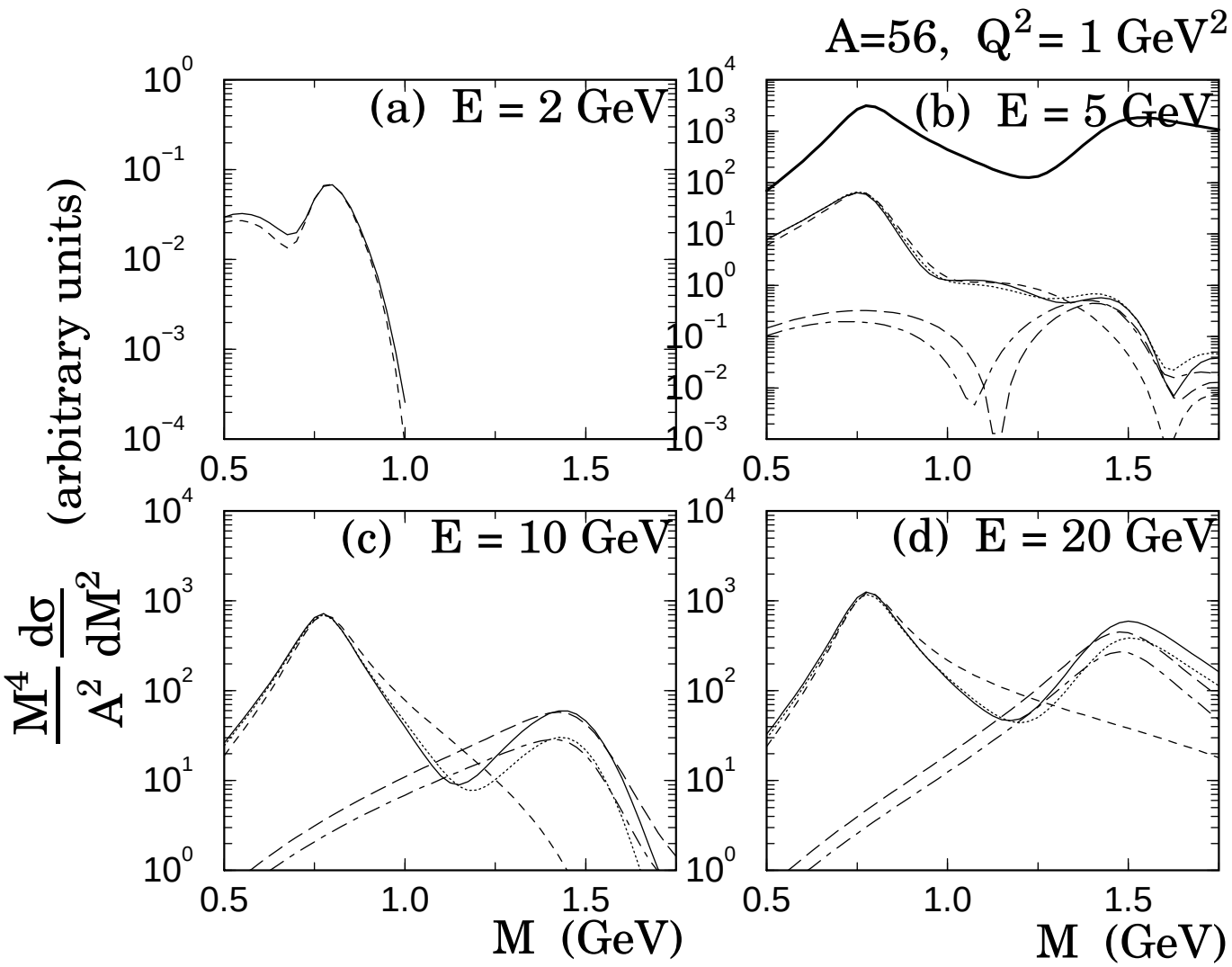
A=56, Q^2= 1 GeV^2
(a) E = 2 GeV
(b) E = 5 GeV
(c) E = 10 GeV
(d) E = 20 GeV
$\frac{M^4}{A^2}\frac{d\sigma}{dM^2}$ (arbitrary units)
M (GeV)
M (GeV)

Fig. 4

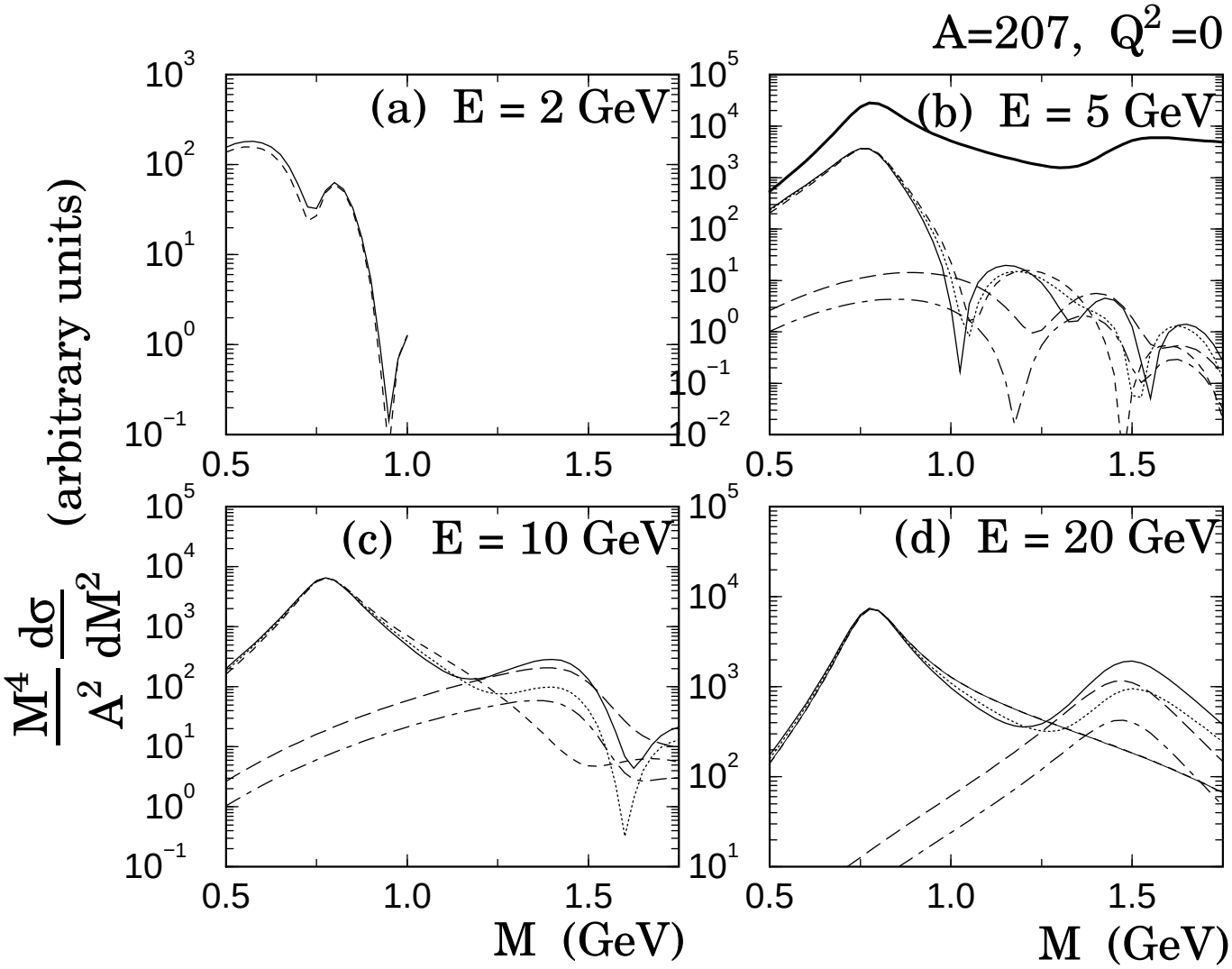
A=207, Q^2=0
(a) E = 2 GeV
(b) E = 5 GeV
(c) E = 10 GeV
(d) E = 20 GeV
$\frac{M^4}{A^2}\frac{d\sigma}{dM^2}$ (arbitrary units)
M (GeV)
M (GeV)

Fig. 5

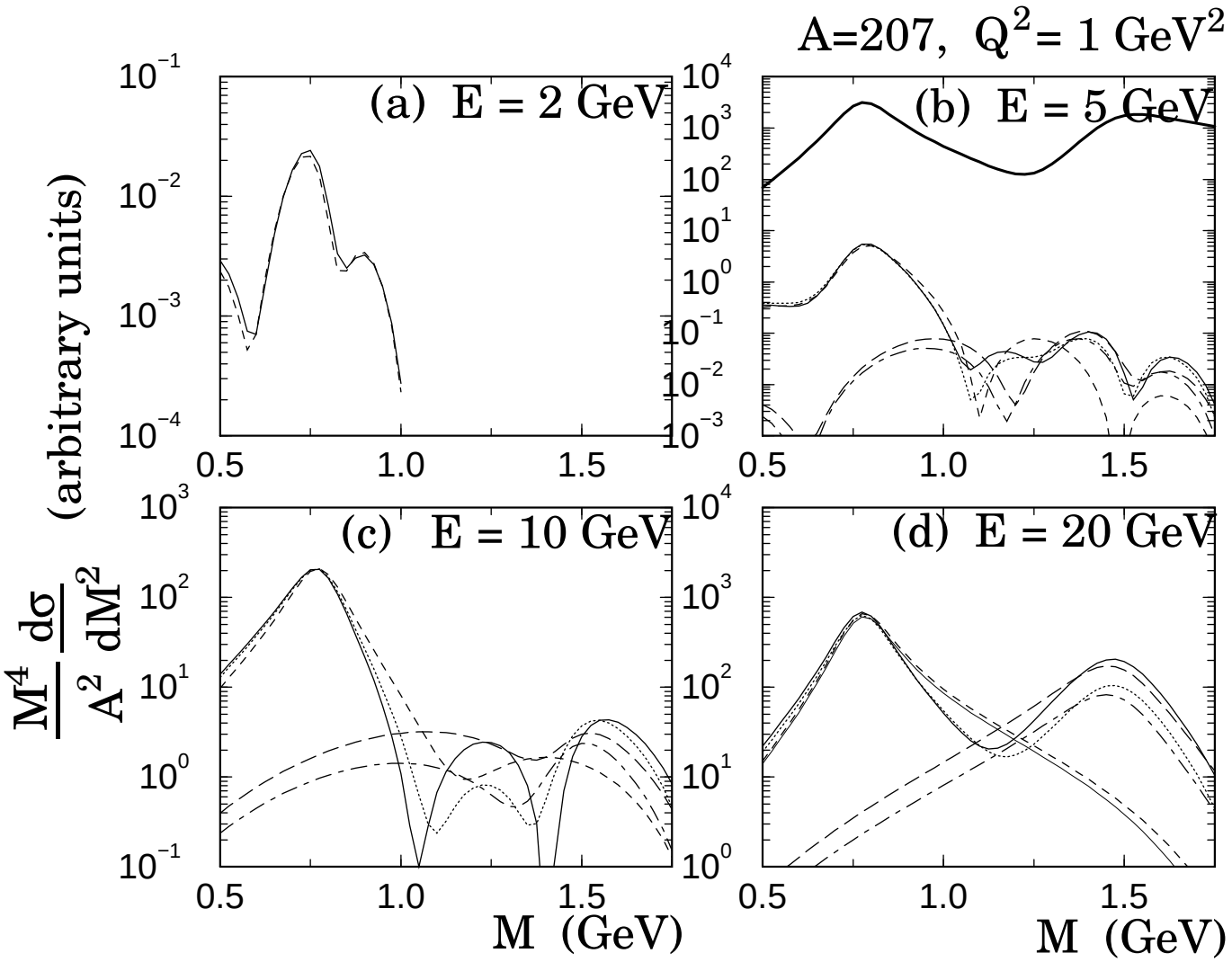
A=207, Q^2= 1 GeV^2
(a) E = 2 GeV
(b) E = 5 GeV
(c) E = 10 GeV
(d) E = 20 GeV
$\frac{M^4}{A^2}\frac{d\sigma}{dM^2}$ (arbitrary units)
M (GeV)
M (GeV)

Fig. 6

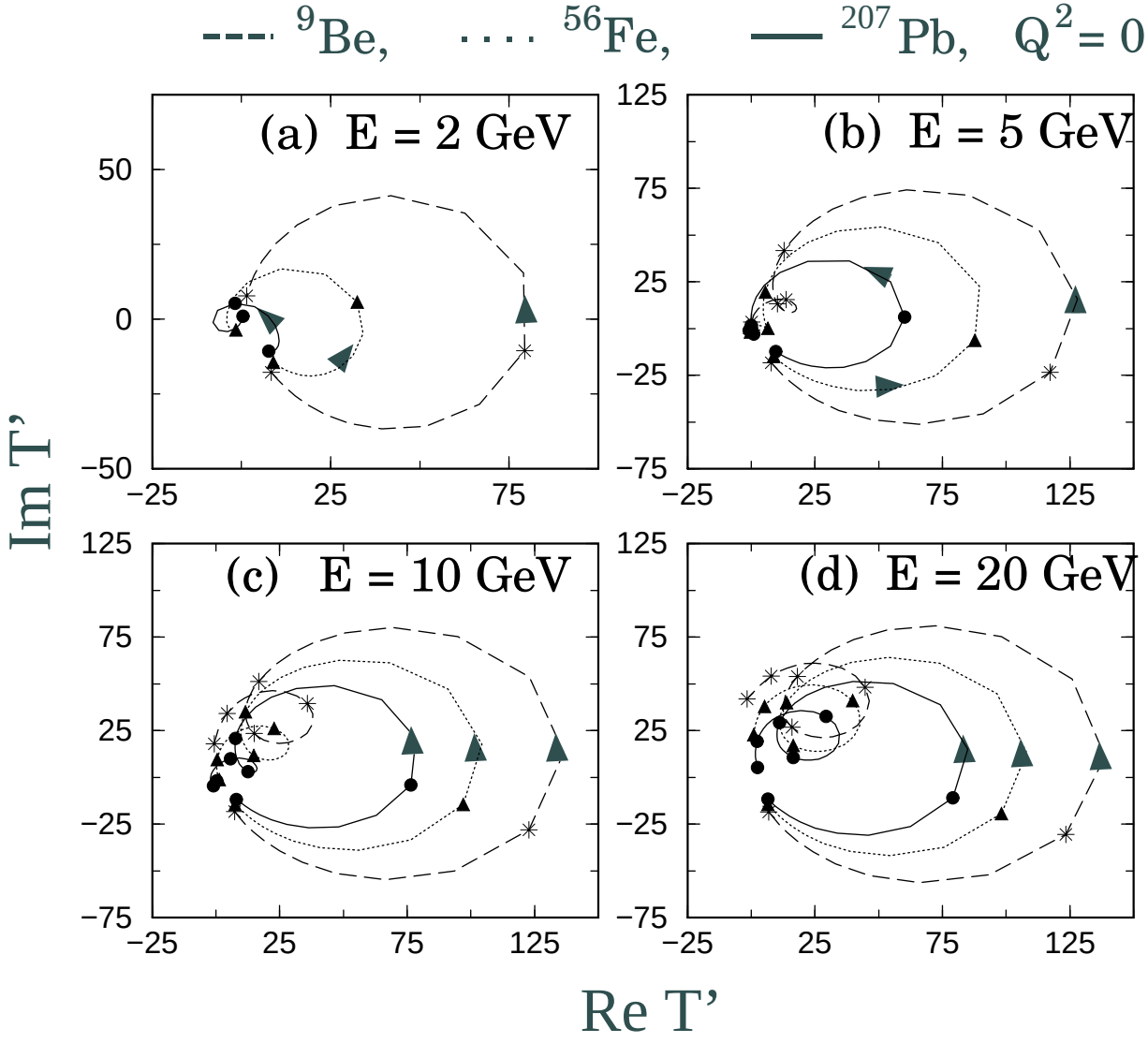

Fig. 8

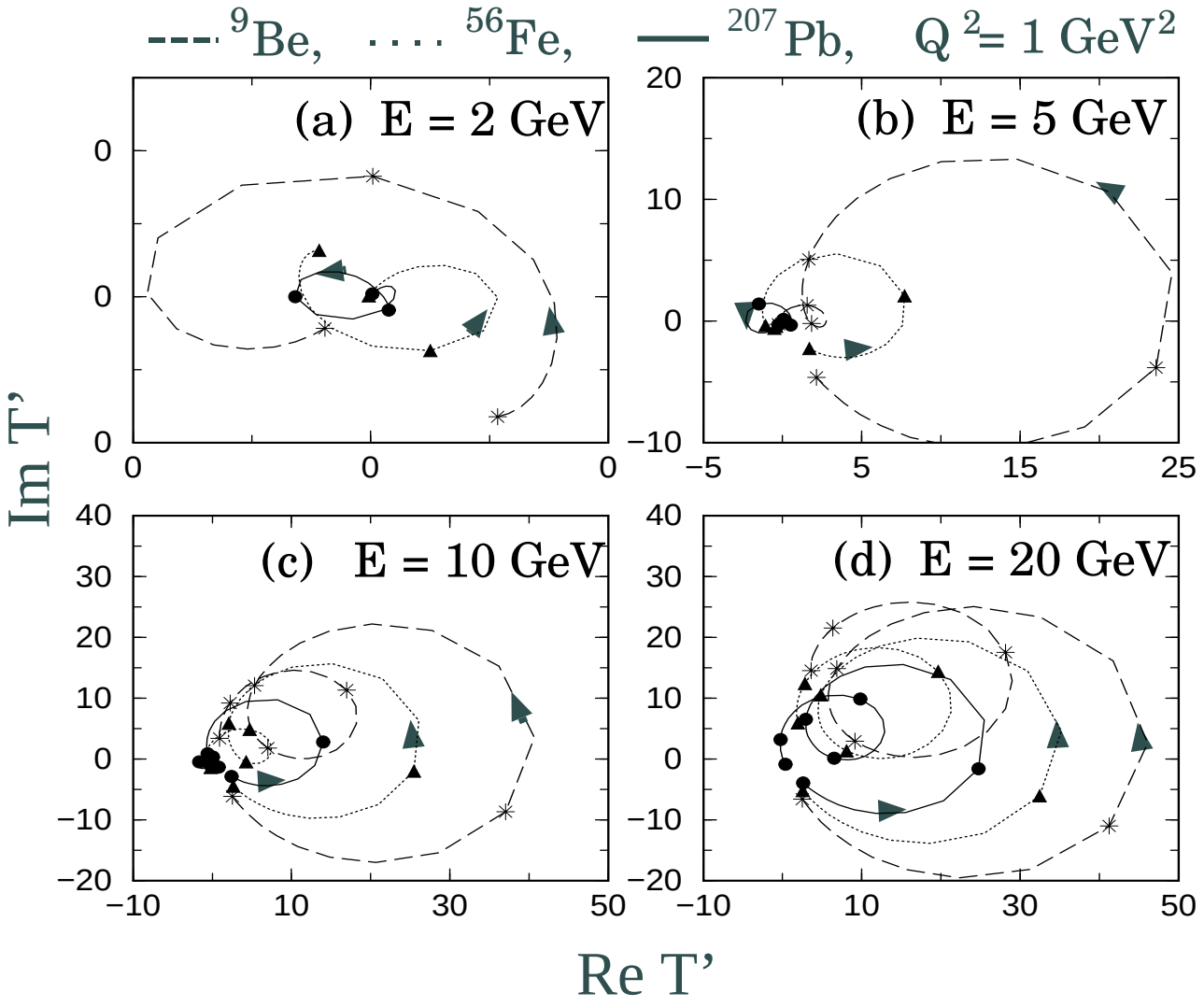
---- ^{9}Be, ... ^{56}Fe, —— ^{207}Pb, Q ^{2}= 1 GeV^{2}
(a) E = 2 GeV
(b) E = 5 GeV
(c) E = 10 GeV
(d) E = 20 GeV
Im T'
Re T'

Fig. 9

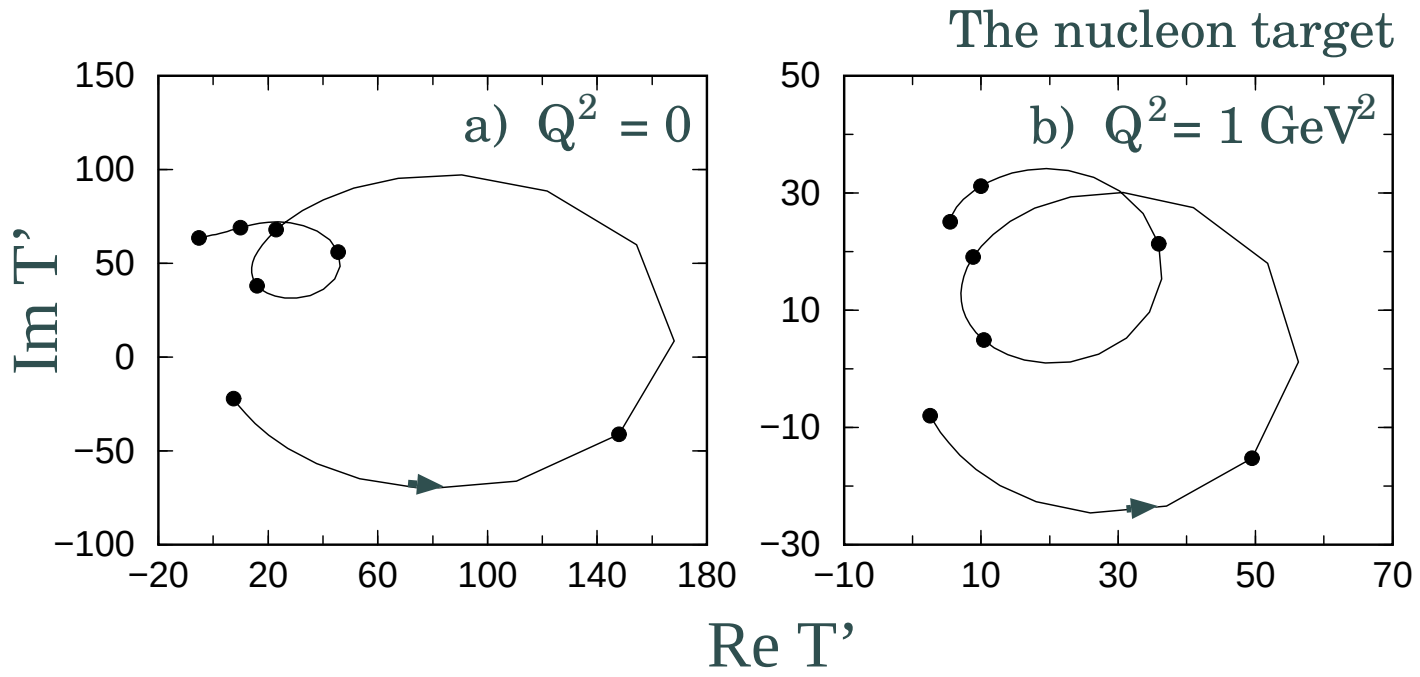
The nucleon target
a) Q² = 0
b) Q²= 1 GeV²
Im T'
Re T'
150
100
50
0
−50
−100
−20
20
60
100
140
180
50
30
10
−10
−30
−10
10
30
50
70

Fig. 7